

## Study on the Aerodynamic Characteristics of a Single-pylon Cable-stayed Bridge Girder by Numerical Simulation and Wind Tunnel Test

Longqi Zhang<sup>1</sup>, Shixiong Zheng<sup>1,\*</sup>, Yu Tang<sup>1</sup>, Hongyu Jia<sup>2</sup> and Yi Bao<sup>3</sup>

<sup>1</sup>School of Civil Engineering, Southwest Jiaotong University, Chengdu, 610031, China

<sup>2</sup>Department of Civil Engineering, Southwest Jiaotong University, Emei, 614200, China

<sup>3</sup>Department of Civil, Architectural, and Environmental Engineering, Missouri University of Science and Technology, Rolla, 65401, USA

Received 12 May 2014; Accepted 15 September 2014

### Abstract

The wind induced vibration is one of the key technical problems for long-span bridge design. Therefore, a study on the aerodynamic characteristics of a single-ylon cable-stayed bridge girder is carried out in this paper. The aerostatic coefficient of the bridge girder, including both construction state and service state, is investigated by wind tunnel test with varying wind attack angle. Then based on the computational fluid dynamics (CFD) method, the flow field around the bridge girder is visualized numerically. The risk of vortex-induced vibration (VIV) is qualitatively evaluated by analyzing the flow features and by considering the Scruton number ( $Sc$ ). Later a dynamic section model is tested in wind tunnel and the VIV phenomenon is observed subsequently. Results show that the aerodynamic stability is assured by the positive slope of the lift coefficient. The VIV response is influenced by the structural damping and the bridge accessory. The amplitude of VIV response can be lower by increasing the structural damping. The maintenance track rail of the bridge girder also does some good for suppressing the VIV as long as the track rail is located at the appropriate place.

*Keywords:* Cable-stayed Bridge with Single Pylon, CFD, Section Model, Static Force Coefficients, Vortex-induced Vibration

### 1. Introduction

The single-ylon cable-stayed bridge usually includes a steel box girder, concrete deck on top, and long lateral arms. This type of bridge is getting increasingly popular in bridge applications due to its various advantages in mechanical performance, effective cost, and appearance. However, these bridges have relatively lower torsion stiffness than other conventional cable-stayed bridges because the cables arranged in the middle of their deck hardly provide sufficient torsion stiffness. Therefore, with bridge spans expanding, the ability to mitigate the wind-induced vibration response with a blunt section girder will raise concerns about proper bridge design [1], [2], [3].

Due to the unique structure of the single-ylon cable-stayed bridge, its structurally dynamic characteristic differs from general bridges. Further, section and aerodynamic performances make results from the section model wind tunnel test different from long-span bridges with a dissimilar section type and thus a different static force coefficient especially vis-à-vis galloping and vortex induced vibration. Past wind resistance studies of single-ylon cable-stayed bridges have usually focused on the streamline box girder [1], [5], [6], [10]. This essay is mainly concerned with VIV performance and its corresponding vibration reducing

measures, which have rarely been mentioned in the literature that focuses on the girder section as the engineering background.

Because of its time efficiency and affordability, the CFD technique has been widely used in wind resistance analysis of bridges, especially for conditions that present wind tunnel tests cannot achieve. Therefore, research on the VIV performance of the engineering structures with CFD has been published widely in the past decades. For instance, Nomura [15], [16] and Wei [17] simulated a vortex-induced vibration of cylinders and the H section pillar by using the ALE finite element method. CAO [18] modelled the interference effects of the cylinder and fluid using the moving-mesh method, which successfully predicted the vortex-induced vibration of the cylinder, Inamura et al [19] calculated the vortex-induced vibration of square columns using a discrete vortex method. Sarwar [20] investigated the mechanism of reduction in the VIV amplitude of a 3D box girder section model by using the 3D large eddy simulations (LES) turbulence model. Hallak [21] analyzed the effects of tall vehicles on the vortex-induced vibration of the Rio-Niteroi Bridge by means of 2D computational fluid dynamics and verified the results using experimental wind tunnel tests. SUN [22] analyzed the force coefficients and flutter derivatives of several long-span deck sections by using both two-dimensional and three-dimensional CFD numerical simulations which were compared with the experimental measurement results.

\* E-mail address: zhengsx@swjtu.edu.cn

## 2. Engineering Background

The single-pylon cable-stayed bridge investigated here is constructed with a steel-concrete composite girder and cables in a single plane. The span layout of the fixed-pier-tower-beam system is 140m+140m, with a 7.5m long concrete beam on each side of the tower. The major span box section girder with a 5.0m-wide box, 10.75m-long lateral arms, 3.0m-arm space, and a 26.5m-wide deck is shown in Fig. 1. Fig. 2 gives the cross section of the steel box girder that employed a single dual-chamber box and the cantilever with a height-variable I shape section. There is no static force coefficient available for reference because of the special bridge structure. Domestic and international standards stipulate that the wind resistance of the bridge needs to be evaluated using a wind tunnel test that has a technical section model.

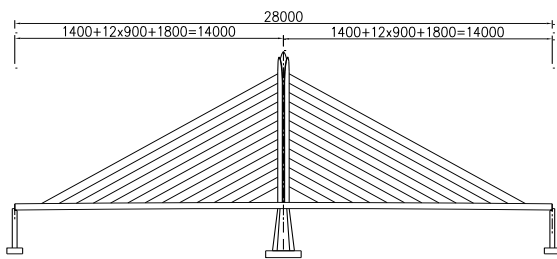


Fig. 1. General arrangement of the bridge (unit:cm)

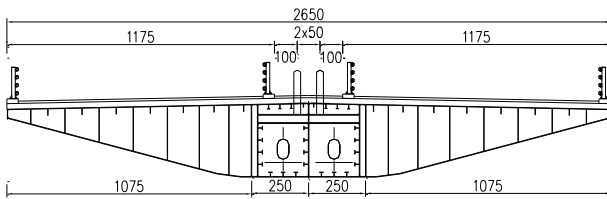


Fig. 2. Cross-section of the girder (unit:cm)

## 3. Static Force Test

### 3.1 Girder Section Model Design

The girder model was 1:50 in scale measuring 2.1m in length, 0.53m in width, and 0.071m in height, and 3.96 of the length-width ratio. The size of the model met the design requirements for wind resistance in the codes [4]. The model was manufactured with wood and plastics to satisfy stiffness and shape. The test was carried out in the second test segment of the Southwest Jiaotong University single-return series duplex wind tunnel (XNJD-1) whose section is a rectangle of 2.4 m (width) × 2.0 m (height).

### 3.2 Static force test result

For the bridge girder, the static wind force can be divided into three components which can usually be expressed as

$$\text{drag } F_H = \frac{1}{2} \rho V^2 H L C_H \quad (1)$$

$$\text{lift } F_V = \frac{1}{2} \rho V^2 B L C_V \quad (2)$$

$$\text{moment } M = \frac{1}{2} \rho V^2 B^2 L C_M \quad (3)$$

Where,  $\rho$ —air density,  
 $V$ —wind velocity,

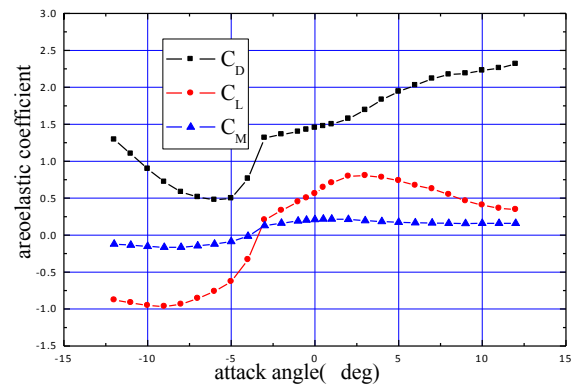
$H$ —height of the model girder,  
 $B$ —width of the model girder,  
 $L$ —length of the model girder.

$C_H, C_V, C_M$  as the drag coefficient, lift coefficient, and moment coefficient of the girder, which can be measured by the wind tunnel test .

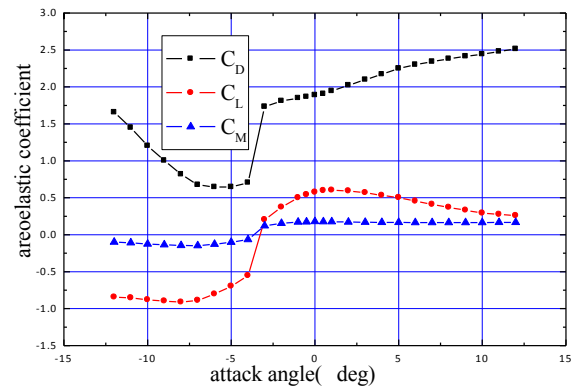
The static force test of the girder proceeded in the uniform flow, with the wind attack angle changing from  $\alpha=-12^\circ$  to  $\alpha=+12^\circ$ ,  $\Delta \alpha=1^\circ$ , and extra  $\alpha=\pm 0.5^\circ$ , in both construction and service states. A photo of the section model in the construction state as it was placed in the wind tunnel is illustrated by Fig. 3. And the graph of the variations of the aeroelastic coefficient with wind attack angle is illustrated in Fig. 4.



Fig. 3. Sectional model of the girder



(a) in construction state



(b) in service state

Fig. 4. Variation of aeroelastic coefficient with wind attack angle

Fig.4 shows the variation rules of the aeroelastic coefficient when the wind attack angles are similar for both the construction and the service states. The drag coefficient

( $C_D$ ) in the service state is slightly larger than the former at  $\alpha=0^\circ$ , for an increased occlusion effect of the railings and the track rails. The slope of the lift coefficient ( $C_L'$ ) of  $C_L-\alpha$  curve is positive. Compared with the larger positive attack angles, the slope of the lift coefficient becomes negative with a small absolute value. The sum of the larger drag coefficient and lift coefficient is above 0, which prevents the girder from galloping. The value of the drag coefficient in the construction state equals 1.5, which is larger than the common streamline steel box girder while  $\alpha=0^\circ$ [6], [13], [14]. Therefore, the cross displacement induced by wind may be unacceptable for construction. Sudden change occurred to the lift and drag coefficients with an attack angle between  $-5^\circ$  and  $-3^\circ$ . Research must focus on the buffeting response for the attack angle  $\alpha=0^\circ$ , which During the buffeting verifications, it may not be the worst condition when the attack angle  $\alpha=0^\circ$ . However, the according buffeting responses due to this case must draw enough attentions.

**4. Preliminary Analysis of the CFD Flow Filed and Vortex-induced Vibration**

Under the condition of the cross wind, the flow direction parallels the lateral steel arms at a distance of 3m. This simplifies the real girder cross section, without arms, making it suitable for a two dimensional field analysis. The simulated computational domain is a rectangle with a length of 12m and a width of 4m. The distance between the girder model and the inlet is 2m and far away from the outlet it is 10m.

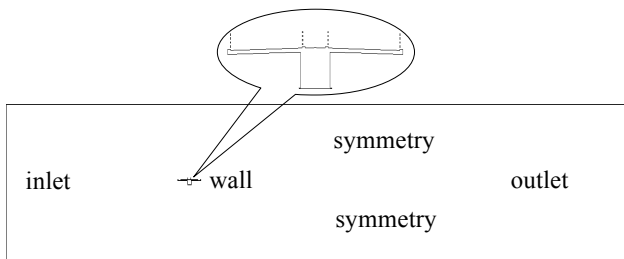


Fig.5. The computational domain diagram

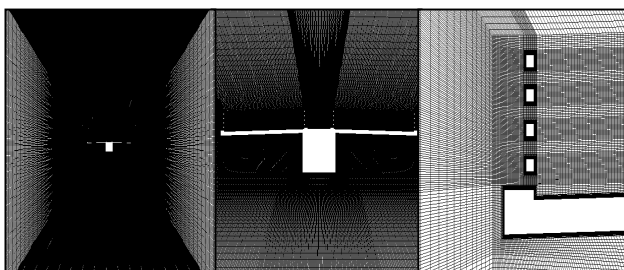
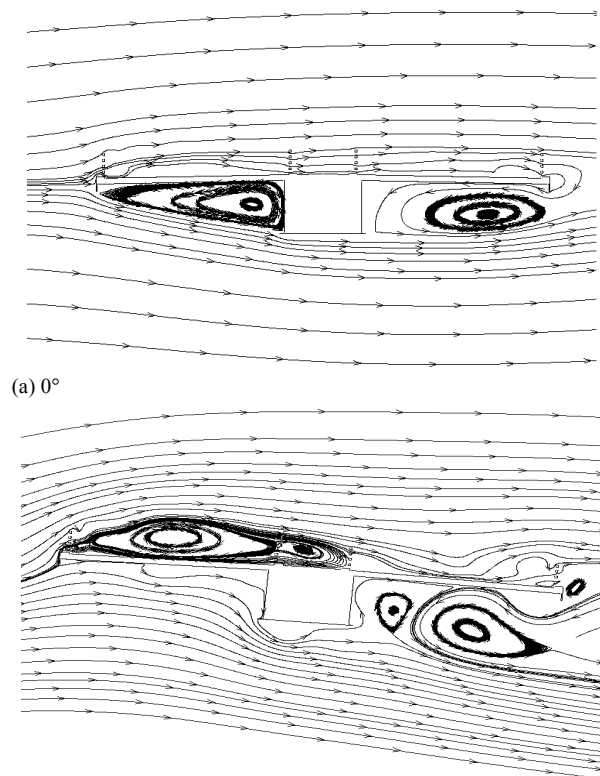


Fig.6. Digital mesh of girder around the girder section

Using the commercial fluid software FLUENT as a computing platform as well as SST  $\kappa-\omega$  turbulence as a model, the flow field around the girder cross section was simulated based on the SIMPLEC algorithm and second-order upwind scheme. At the same time, the two dimensional unsteady incompressible flow solver is used to solve the fluid equations. Streamline charts of the girder in the service state is illustrated in Fig 7.



(a)  $0^\circ$   
(b)  $+3^\circ$   
Fig.7. Streamline charts of the girder in service state

Attack angle  $\alpha=0^\circ$ (Fig.7a)

The wind that flows through railings generates small scale vortices above the deck due to the shunt effect on the front of the deck and the grid occlusion accelerating effect. There is a negative pressure region behind the railings for flow separation, which is attached to the deck not far downstream. At the same time, no obvious large scale eddies form above the bridge deck.

Large scale eddies form on both sides of the box girder behind the deck. There are two possible reasons for the formation of large eddies near the windward side. On the one hand, the original horizontal moving flow that is directly blocked by the girder makes the static pressure stronger and causes an adverse pressure gradient downstream. On the other hand, due to the whole exiting deck, the flow below the windward side of a certain area is located within the separated shear layers that are formed in front of the deck. Due to the shunt effect of the box girder, the flow around its bottom also increases the static pressure and, as a result of the expansion of the shear boundary layer and friction, the adverse pressure gradient, backflow, and eddies are formed on the leeward side of the box girder.

Seen spatially, the eddy scale size on both sides of the box girder approximates the feature size of the box girder, which makes the eddy energy concentrate in a relatively low frequency and which may increase the possibility of the vortex-induced vibration of the girder. The two eddies rotate counterclockwise below the deck and some of their moment effect to the bridge cancels each other out, while the concentrated force (such as lift) may be larger due to the superposition effect of two eddies. So that the girder may be prone to the vertical vortex-induced vibration at  $\alpha=0^\circ$ . In the meantime, since the eddy on the left side is larger than that on the right side, vortex-induced torsion vibration is hence generated as the result of the different composite force.

Attack angle  $\alpha=+3^\circ$ (Fig.7b)

Above the bridge deck, the large scale eddies are generated on the upwind side due to the deck's shunt effect and the mainstream will not re-attach until it is far from the downstream.

Due to the direct effect of positive attack angle wind on the box girder windward side, large scale eddies can not be formed under the bridge deck as a result of the blown-off shear separation layer in front of the deck by the mainstream. However, if the formation conditions are unaffected, large scale eddies can still be formed on leeward side of the box girder.

In terms of the correlation of large scale eddies, the eddies on the deck and behind the box girder are both located in the wake region of the girder section at attack angle  $\alpha=+3^\circ$  and their correlation is larger than the eddies formed at attack angle  $\alpha=0^\circ$ . Furthermore, it is possible that behind the alternate cycle, a similar cylindrical shedding vortex might come up, which is disadvantageous for vortex-induced vibration.

When the structural damping ratio is 0.3% and  $Sc$  is both in construction ( $Sc=9$ ) and in service ( $Sc=13$ ), below 20, there is a possibility of vortex-induced vibration[12].

Through the analysis of the flow field around the girder and with the estimated  $Sc$  number, the bridge is more likely to occur vortex-induced vibration, which needs clarification by a wind tunnel test.

### 5. Dynamic Tests and discussions

#### 5.1 Dynamical test model

The dynamic test section model, suspended on the scaffold by 8 extended springs, forms two-degree freedom vibration systems of vertical movement and rotation around the model axis. The natural frequency parameters of the bridge in the construction and service state are listed in table 1.

Table 1. Natural frequency of the bridge

Case	Real bridge(Hz)		Section model(Hz)	
	vertical $f_v$	torsion $f_t$	vertical $f_v$	torsion $f_t$
In construction state	0.2633	0.6711	3.115	7.939
In service state	0.6192	1.0727	5.81	10.10

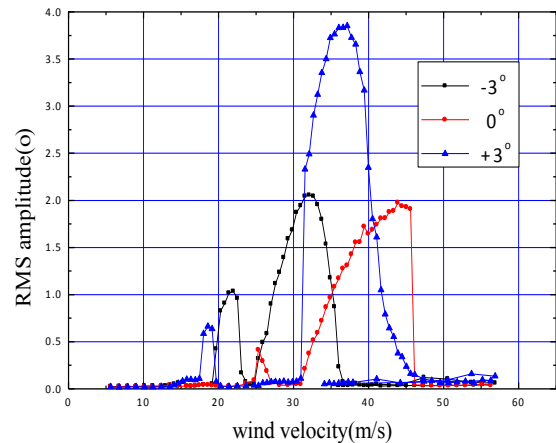


Fig.8. The dynamic sectional model

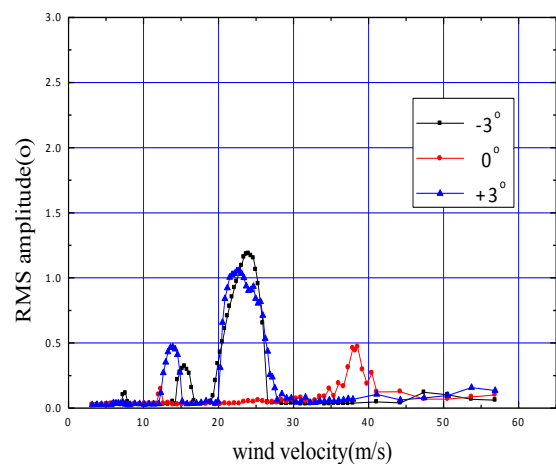
#### 5.2 Vortex-induced vibration test

For long-span bridges with light weight and low damping, when air flows through the girder section, the alternating

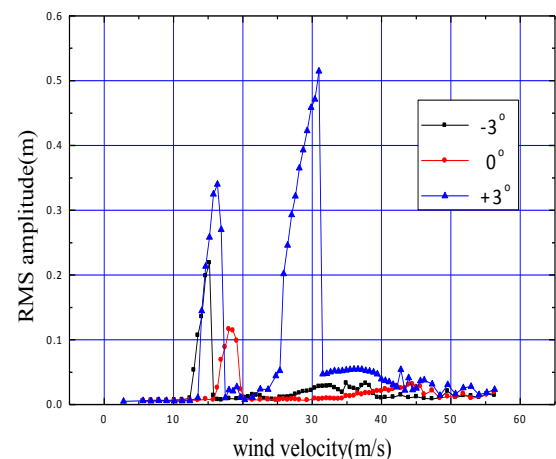
cyclical shedding eddies will cause vortex-induced vibration[7]. A composite bridge girder with steel box and large lateral arms has a blunt section. VIV performance research has not been conducted for this type of bridge. Figures 9 and 10 show the curvatures between vertical/torsional VIV amplitude and the wind speed of the target bridge in both the construction state and the service state under various damping conditions. According to prior research, the VIV amplitude can be decreased [7], [8], [9] by changing the damping ratio and by moving the maintenance track rail on the bridge. In the figures,  $D=8m$ ,  $D=10m$  signify the distances from the maintenance track rail location to the center axis of the girder as 8m, 10m, respectively.

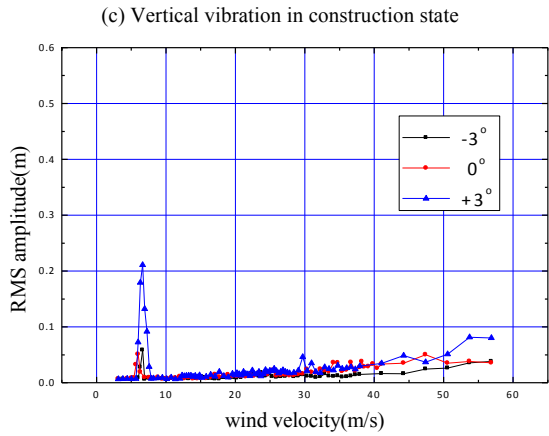


(a) Torsional vibration in construction state



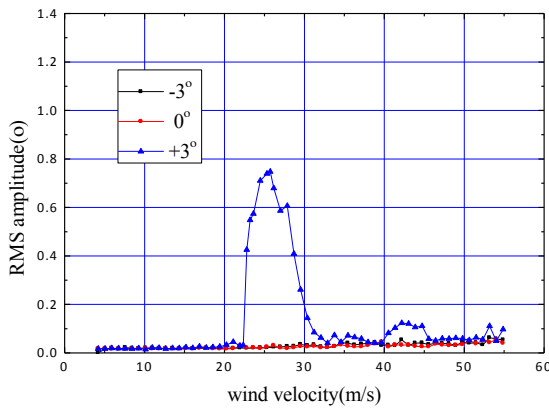
(b) Torsional vibration in service state



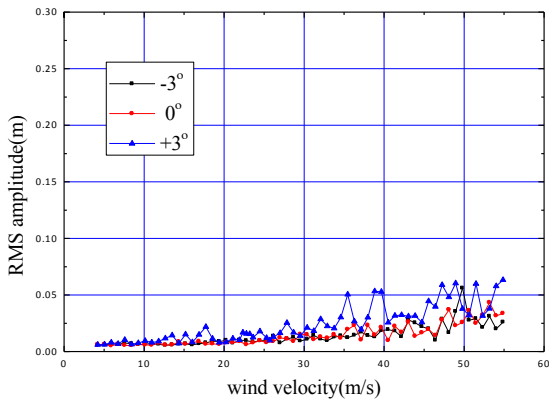


(d) Vertical vibration in service state

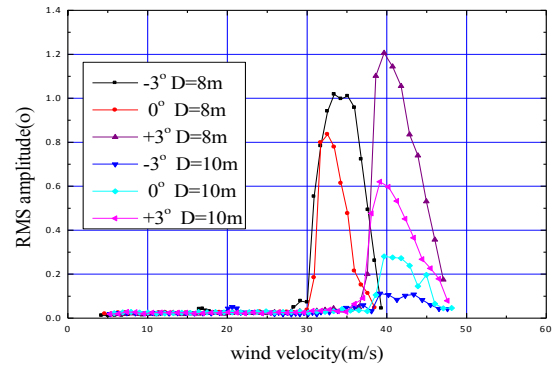
Fig.9. VIV amplitude of real bridge with small damping ratio( $\zeta=0.003$ )



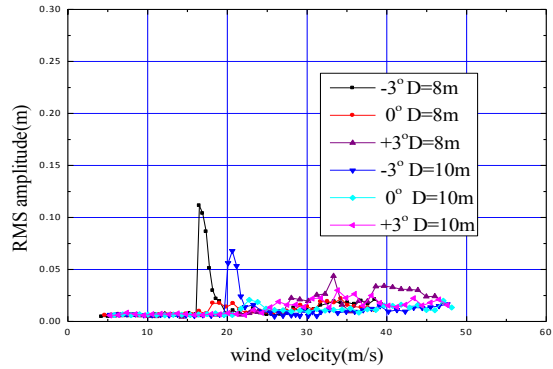
(a) Torsional vibration in construction state



(b) Vertical vibration in construction state



(c) Vertical vibration in service state



(d) Torsional vibration in service state

Fig.10. VIV amplitude of real bridge with larger damping ratio ( $\zeta=0.01$ )

It can be concluded from Table 3 and Fig. 9 that the vertical and torsional VIV is subtle when the bridge is in the construction state with a small damping ratio ( $\zeta=0.003$ ), wind attack angle  $\alpha=0^\circ$ , but obvious when  $\alpha=+3^\circ$ . The CFD simulation analysis coincides with the conclusions from the former section that when the bridge is in the service state and  $\alpha=0^\circ$  the torsional vibration lacks a locked vertical vibration. Moreover, when  $\alpha=+3^\circ$ , the torsional VIV amplitude and the maximal vertical VIV amplitude increases sharply. At the same time, the vertical and torsion VIV are coupled to a certain extent and they are not absolutely separated. The VIV results from the wind tunnel test are relatively close to the CFD flow field simulation in the previous section, which explains the mechanism of the vortex shedding around the girder to the torsional VIV. The comparisons verify the feasibility of using CFD to simulate the flow field and judge the VIV of the bridge structure with a preliminary blunt section.

Table 2. VIV experiment results of the girder

Case attack angle( $^\circ$ )	Locked wind velocity(m/s)		Peak amplitude		Damping ratio $\zeta$	
	vertical	torsion	vertical(mm)	torsion( $^\circ$ )		
In construction state	-3 $^\circ$	6.3~6.9	14.5~16.4 19.6~25.9	58.4	1.19	0.003
	0 $^\circ$	5.7~6.3	36.0~44.2	50.0	0.47	0.003
	+3 $^\circ$	5.7~7.6	12.3~14.8 20.2~28.4	210.8	1.06	0.003
In service state	-3 $^\circ$	12.9~15.8	19.7~23.1 25.3~36.0	218.4	2.1	0.003
	0 $^\circ$	16.3~19.7	25.3~26.5 31.5~41.6	116.2	2.0	0.003
	+3 $^\circ$	13.5~19.1 22.5~31.5	17.5~19.1 31.0~47.3	514.6	3.9	0.003

The peak amplitudes of the vertical and torsional VIV in the service state are larger than in the construction state at the same attack angle, while the wind velocity of the beginning vibration in the construction state is relatively lower than the service state. This phenomenon is possibly explained by the fact that the general equivalent mass of the girder in the construction state is smaller than when it is in service state, and that it is more easy to break the original static state of inertia for a vortex-excited force. On the other hand, the railings and maintenance track rails installed on the bridge change the flow field distribution around the girder, which also makes the vortex shedding position and range change. Requirements for the bridge operation and traffic safety could not be met and effective measures to suppress vibration is needed, because the resonance wind speed is partly less than the corresponding design wind speed while the vertical or torsional VIV amplitude exceed the wind specification.

Because of the vibration energy dissipation effect in the process of damping, after increasing the damping ratio to 1%, torsional VIV occurs in the construction state only when the attack angle  $\alpha=+3^\circ$ . Compared with the state of the small damping ratio (0.3%), the VIV amplitude decreases significantly while the wind velocity of the beginning vibration increases with no vertical VIV. For the bridge in the service state, at different attack angles, the torsional VIV amplitudes increases when the distance between the bridge maintenance and the midline bridge of 8m are all larger than the displacement between the maintenance track rail and the bridge axis as 10m. Vertical VIV occurs at attack angle  $\alpha=-3^\circ$  in both the construction and the service state, and the rules of vibration amplitude with wind velocity are similar to the torsional vibration. It is helpful to diminish the VIV amplitudes by moving the maintenance track rail outward 10m away from the bridge axis. From the analysis of the charts of VIV amplitude with wind velocity, it can be obtained that at the state of the same damping ratio, the torsional VIV happens more feasibly or has a larger relative

amplitude in both the construction and service states, with torsional vibration only occurring in some situations. The relatively lower torsional frequency, mainly due to the unique bridge section and the single tower and single cable-plane, may tend to cause torsional VIV easily.

## 6. Conclusions

Through the experimental analysis of the static and dynamic section model wind tunnel tests under multi-loading conditions and the CFD numerical simulation of a single pylon cable-stayed bridge, conclusions are made as follows. A larger drag coefficient may produce more significant static wind-induced displacement. It is more likely to generate torsional VIV when the single cable plane cable-stayed bridge with single pylon has a section of box girder with big lateral cantilever arms. CFD numerical simulation shows that there is a possibility of VIV of the girder. At the same time, the mechanism of VIV induced by the eddies shedding is clearly illustrated by the streamlines distribution in the flow filed and is further verified by the corresponding segment wind tunnel test. The vertical and torsional VIV occurs when the damping ratio is small ( $\zeta=0.003$ ) in both the construction and the service state. If the damping ratio increases to  $\zeta=0.01$ , VIV can be restrained by moving the position of the maintenance track rail.

## Acknowledgement

This work was supported by the National Natural Science Foundation of China under NO. 51378443 with Professor Shixiong Zheng as the program director, supported by the National Natural Science Foundation of China under Grant No.51308465 and supported by Scientific and Technological Innovation Foundation of China under Grant No. 2682014CX004EM.

## References

- [1]. LIU Z.-W., XIN Y.-b., CHEN Z.-Q., Sectional model wind tunnel tests and analysis of cable-stayed bridge with single pylon and single cable plane, *Journal of Hunan University (Natural Sciences)*, 36(10), 2009, pp. 7-12. (in Chinese)
- [2]. WARDLAW R L. Sectional versus full model wind tunnel testing of bridge road decks, *Proc Indian Acad Sci*, 3(3),1980, pp.177-198.
- [3]. Xiang H.-F., Modern theory and practice on bridge wind resistance, Beijing: *China Communications Press*, 2005. (in Chinese)
- [4]. Ministry of Transport of the People's Republic of China. JTG/TD 61-01-2004 Wind-resistant Design Code for Highway Bridges Beijing: *China Communication Press*, 2004.(in Chinese)
- [5]. Tanaka.H. Similitude and modeling in bridge aerodynamics: Aerodynamics of large bridges, Rotterdam: *Balkema*, 1992.
- [6]. Hu F.-Q., Chen A.-R., Lin T.-L., Experimental investigation on wind-resistant behavior of the single-tower cable-stayed bridge over south channel of Hangzhou gulf, *Engineering Mechanics*, 23(8) ,2006, pp.132-137.(in Chinese)
- [7]. SUN Y.-G., LIAO H.-L., LI M.-S., Mitigation measures of Vortex-Induced Vibration of suspension bridge based on section model test , *Journal of Southwest Jiaotong University*, 47(2), 2012, pp.218-224.(in Chinese)
- [8]. XIAN R., LIAO H.-L., LI M.-S., Analysis of vortex-induced vibration of large-scale section model of girder in wind tunnel , *Journal of Experiments in Fluid Mechanics* , 23(4) , 2009, pp.15-20(in Chinese)
- [9]. MENG X.-L., ZHU L.-D., DING Q.-S., The location of maintenance truck implications of Semi-closed double separation box bridge vortex vibration performance [C] *The 15th National Conference on Structural Wind Engineering Academic Conference Symposium. Beijing: China Communication Press*, 2009, pp.157-162.(in Chinese)
- [10]. HE X.-D., et al., Wind tunnel test study on wind-induced internal force of a cable-stayed bridge tower , *Journal of Southwest Jiaotong University*, 35(5), 2000, pp.471-474.(in Chinese)
- [11]. Robinson R. W, Hamilton J.A Criterion for Assessing Wind Induced Cross flow Vortex Vibrations in Wind Sensitive Structures, *Health and Safety Executive-Off-shore Technology Report, London*: 1992.
- [12]. Claes Dyrbye, Svend Ole Hansen. Wind Loads on Structures, *John Wiley & Sons Ltd*, 1997.
- [13]. ZHOU Q., ZHOU Z.-Y., GE Y.-J., Mode and mechanism of aerostatic stability for suspension bridges with double main spans. *Journal of Harbin Institute of Technology*, 44(8), 2012, pp.76-82.(in Chinese)
- [14]. CHENG J., XIAO R.-C., XIANG H.-F., Full range nonlinear aerostatics analysis for long-span cable-stayed bridge. *China Journal of Highway and Transport*, 13(3), 2000, pp.25-28.(in Chinese)
- [15]. Nomura T., Finite element analysis of vortex-induced vibrations of bluff cylinders , *Journal of Wind Engineering and Industrial Aerodynamics*, 46 & 47, 1993, pp.587-594

- [16]. Nomura T., A numerical study on vortex-excited oscillations of bluff cylinders, *Journal of Wind Engineering and Industrial Aerodynamics*, 50, 1993, pp. 75-84.
- [17]. R.Wei, A.Sekines, M.Shinura. Numerical analysis of 2D vortex-induced oscillation of a circular cylinder, *International Journal for Numerical Method in Fluids*, 21 (3), 1995, pp. 993-1005.
- [18]. CAO F.-C., XIANG H.-F., Calculation of unsteady flow around circular cylinder and vortex-induced vibration, *Journal of Hydrodynamics*, 16(1), 2011, pp.111-118.
- [19]. T Inamuro, T Adachi, H Sakata. Simulation of aerodynamic instability of bluff body, *Journal of Wind Engineering and Industrial Aerodynamics*, 46&47, 1993, pp. 611-618.
- [20]. Sarwar M.W., Ishihara T., Numerical study on suppression of vortex-induced vibrations of box girder bridge section by aerodynamic countermeasures, *Journal of Wind Engineering and Industrial Aerodynamics*, 98(12), 2010, pp.701-711.
- [21]. Hallak P.H, Pfeil M.S, Oliveira, Serigo R C, et al. Aerodynamic behavior analysis of Rio-Niteroi bridge by means of computational fluid dynamics, *Engineering Structures*, 56, 2013, pp.935-944.
- [22]. Bai Y.-G., Yang K., Sun D.-K., et al., Numerical aerodynamic analysis of bluff bodies at a high Reynolds number with three-dimensional CFD modeling, *Science CHINA-Physics Mechanics & Astronomy*, 56(2), 2013, pp.277-28.